(66)

APPLICATIONS OF HIGH INDIUM CONTENT InGaAs/AlGaAs QUANTUM WELLS IN THE 2–7 μm REGIME

E.L. Martinet, B.J. Vartanian, G.L. Woods, H.C. Chui, J.S. Harris, Jr., M.M. Fejer.
Center for Nonlinear Optical Materials, Stanford University, McCullough 226, Stanford CA 94305-4055

B.A. Richman, C.A. Rella.
W.W. Hansen Laboratory of Physics, Stanford University, Stanford CA 94305-4085

ABSTRACT: We report on some applications of high indium content quantum wells for mid–infrared (2–7μm) applications. Studies have been done to explore intra–valence band absorption in the mid–infrared between valence band hole states. Second harmonic generation spectroscopy is demonstrated in the conduction band near 5.5 μm.

1. Introduction

Until recently, intersubband phenomena in the mid–IR (2–7μm) regime have remained largely unexplored because of both the lack of semiconductor materials presenting sufficient bandgap engineering possibilities to create useful resonances and the lack of tunable high power sources in this wavelength region for characterization. The introduction of high indium content (HIC) InGaAs/AlGaAs quantum wells (QW)[1], together with the development of free-electron laser (FEL) facilities[2] uncover a new field of experiments in the mid–IR. We have recently demonstrated HIC–QWs with intersubband transition resonances out to 2.1μm, due to large band offsets in the conduction band (up to 1.4eV) and low effective mass.[3-5] HIC structures can be realized by reducing epilayer strain with a graded buffer[1]. This enables one to increase the range of bandgap engineering to highly strained systems in order to design a well geometry that optimizes the linear or nonlinear reponse of the system at a given transition energy. We demonstrate normal incidence absorption from heavy- to light- holes in *p*–doped HIC–QWs at 4.13μm. We also report the measurement of the second order nonlinear susceptibility ($\chi^{(2)}$) of asymmetric QWs as a function of detuning from the near double resonance (5.5μm to 3μm) using a FEL.

2. Intra–Valence Band Transitions

To date, most work on intersubband absorption in QWs has concentrated on the conduction band (CB) using *n*–doped QWs. However, due to the symmetries involved with electron states in the conduction band, a component of the polarization of the incident radiation normally must lie in the growth direction of the QWs in order to effect a transition. Most often, this is

H. C. Liu et al. (eds.), Quantum Well Intersubband Transition Physics and Devices, 261–273.
© 1994 *Kluwer Academic Publishers. Printed in the Netherlands.*

done by orienting the sample at Brewster's angle to maximize the z component of light in the QWs. Methods have been found to surmount this difficulty by, for example, grating coupling into a waveguide. Normal incidence absorption has been observed in n–type X or L valley QWs, but these transitions are limited by the shallow wells depths to the far-IR[30]. For holes, however, the symmetry selection rules are different. Due to the mixing of the heavy– and light– hole states away from the Brillouin zone center[6] interactions between mostly heavy– and mostly light– hole like mixed states (henceforth referred to as heavy– and light– hole states) are allowed for light propagating in the growth direction as previously shown by Levine[7]. This enables one to achieve normal incidence absorption without the use of gratings or other techniques[8-12]. Since HIC–QWs have large valence band offsets ΔE_V, transitions in the mid–IR are possible. With the use of p–doped HIC–QWs, we demonstrate normal incidence absorption in the 3–5μm atmospheric window for normal incidence photodetector and modulator applications.

Since these HIC–QWs are highly strained, there is some difficulty in accurately predicting the band edge profile and energy levels. The problem is especially acute in the valence band, where the strain results in heavy hole–light hole band edge splitting and electronic state mixing. As a result, prior to making devices, one must first do a fair amount of characterization to determine the energies of the levels, the dipole matrix elements, and the effect of the residual strain on the heavy hole–light hole band edge splitting. To this end, we have designed and grown several sets of QWs to accurately determine the effects of such variables as: barrier thickness, well thickness, doping concentration, and dopant location (well or barrier).

The structures we used were 50 HIC-QWs all grown on (100) semi-insulating GaAs substrates by molecular beam epitaxy. The InGaAs/AlGaAs HIC–QWs had a 50% indium concentration in the wells[13] and a 45% aluminum concentration in the barriers. The absorption measurements were made on a Bruker Fourier transform infrared spectrometer using three different geometries: Brewster's angle (73° for GaAs) with TM incident, Brewster's angle with TE incident, and normal incidence (NI). The TM geometry has a component of the incident electric field in the direction of growth and is commonly used for intra–conduction band absorption, whereas the TE and NI geometries confine the direction of the electric field to the plane of the QW.

For the TE and NI measurements, a reference sample with a structure identical to the sample but without carriers was necessary to compensate for the multiple reflection effects from the QW epilayers. The difference between using such a reference sample rather than a GaAs substrate is marked. Without the epilayers included in the reference sample, etalon fringes completely mask the intra–valence band absorption. For our reference sample, we used an undoped structure, grown immediately preceding the doped samples. Measurements were also made on a QW sample, where the reference sample was a proton bombarded portion of the doped QW sample. It has been shown previously[14] that proton bombardment creates deep levels which trap the carriers in n–doped QWs making them unavailable for intra–conduction band excitation. We compared a proton bombarded p–doped sample to an undoped reference and saw that the absorption peak also disappeared.

The QW samples were grown on a graded InGaAs buffer layer with the same type of optimized structures we found for HIC conduction band QW structures[15]. The well was Be doped to $p = 1 \times 10^{19}$ cm^{-3}, and the InGaAs buffer was graded to a maximum indium concentration of 17%. In figure 1, we show the absorption spectra from a 40Å $In_{0.5}Ga_{0.5}As$ well with 80Å $Al_{0.45}Ga_{0.55}As$ barriers for all three geometries, TM, TE and NI. As can be seen from the figure, there is a transition in all three geometries at very nearly the same energy. Because there is absorption at normal incidence, the transition is between heavy and light hole states. The magnitude of the transition is smaller than for similarly doped n-type QWs, but we can compensate for this by doping the valence band higher than is possible in the conduction band. This will be discussed in section 2.3.

2.1. BARRIER WIDTH VARIATION

We performed a study to determine the effect of barrier thickness on the energy and the strength of the transition. Assuming the QWs and barriers had some effective combined strain relative to the buffer layer, then changing the proportion of the barrier to well thickness should change the strain in the well. This would result in a different band profile due to the resultant strain splitting.

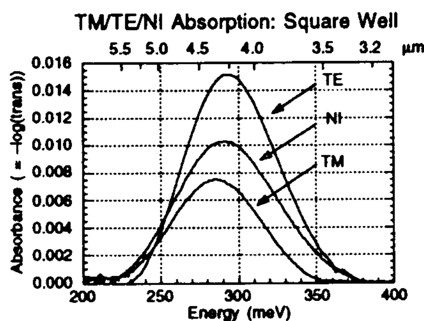

Figure 1
Absorption spectra of square well samples at Brewster's angle TM and TE polarizations and at normal incidence. Well: 40Å $In_{0.5}Ga_{0.5}As$; $p = 1 \times 10^{19}$ cm^{-3} throughout the well. Barrier: 80Å $Al_{0.45}Ga_{0.55}As$.

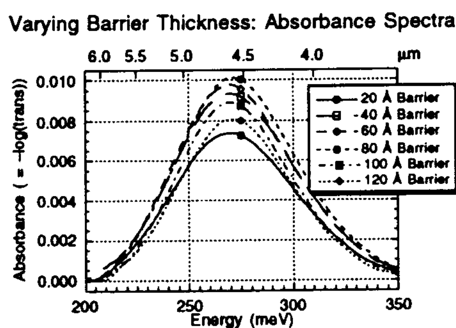

Figure 2
Absorption spectra of 40Å quantum wells doped $p = 1 \times 10^{19}$ cm^{-3} throughout the well. Buffer graded from $In_{0.015}Ga_{0.985}As$ to $In_{0.3}Ga_{0.7}As$. Barrier thickness varies from 20 to 120 Å $Al_{0.45}Ga_{0.55}As$.

We grew a series of 40Å $In_{0.5}Ga_{0.5}As$ QWs varying only the $Al_{0.45}Ga_{0.55}As$ barrier thickness. In each sample, the QW was p-doped with Be to $p = 1 \times 10^{19}$ cm^{-3}. Also, the buffer was graded from 1.5 to 30% indium. The absorption spectra are shown in figure 2 and were obtained by making Brewster's angle measurements with TM radiation. A GaAs substrate was used as a reference. As can be seen from the plot, there is almost no shift in the position of the peak at 270 meV. However, the strength of the absorption is affected. The integrated absorption fraction (IAF) is a maximum with 80Å barriers: 5.82 Abs-cm^{-1}. This is 11% larger than the average IAF seen for these samples. These results indicate that if the

strain were changing as the barrier thickness is varied, the change has little or no discernible effect on the position of the hole energy levels relative to each other, implying that the band edge profile also remains unchanged.

2.2. WELL WIDTH DEPENDENCE

We examined the well width dependence of the intra-valence band absorption energy by growing several $In_{0.5}Ga_{0.5}As$ QW samples of varying well width. In each, the barrier was 50Å $Al_{0.45}Ga_{0.55}As$, and the buffer was graded from 1.5 to 30% indium composition. As before, the entire QW was doped with Be to $p = 1 \times 10^{19}$ cm^{-3}. However, unlike the varying barrier thickness study, in this case, the total sheet charge density changes since, with uniform doping, it is directly proportional to the well width.

We see in figure 3a that the transition energy reaches a peak in the 27Å well, and then begins to drop again as the wells get narrower. This indicates that the upper level rises more rapidly than the lower level for the wider wells, as is expected for a lighter mass hole. For even narrower wells, however, the upper level is no longer rising as rapidly and is effectively "pinned" at the top of the well. This is because the upper state is now more delocalized and is mostly in the barriers, making it virtually unaffected by well width variations. Figure 3b shows how the absorption rises with well width while the full width half maximum (FWHM), decreases. The increase in the FWHM with decreasing well width is probably due to interface scattering. It may also be due to the change in the nonparabolicity of the bands in k-space as the well width varies[16, 17]. In addition, the total absorption rises, in general, as the well width increases. This would be affected by two factors: the number of carriers available for absorption and the dipole matrix element between the two states involved since the magnitude of the absorption is directly related to both of these.

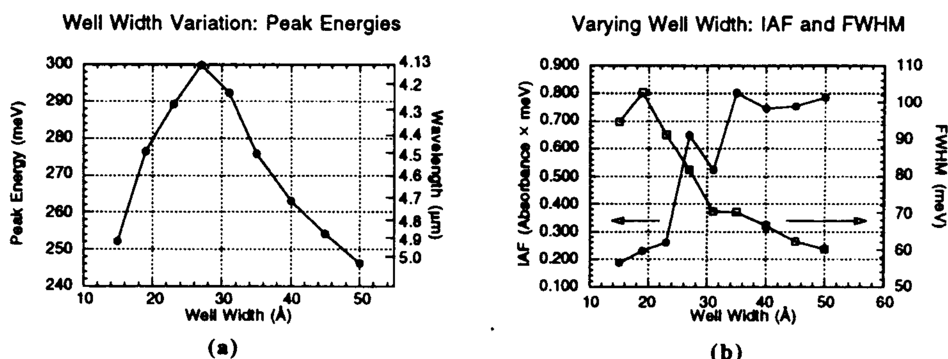

Figure 3

Well widths vary from 15 to 50Å. The QWs are doped $p = 1 \times 10^{19}$ cm^{-3} throughout the well. The barrier is 50Å $Al_{0.45}GaAs_{0.55}As$ and the buffer is graded from 1.5 to 30% indium. a) Peak energies for QWs as a function of the well width. b) IAF and FWHM vs. well width.

2.3. DOPING DEPENDENCE

Figures 4 (a) and (b) show the results of a study on the effects of doping on the peak position and IAF for the three geometries used. We use two different doping configurations: one in which the well is doped and the other with the barrier doped. The QWs consist of 45Å $In_{0.50}Ga_{0.50}As$ with 50Å $Al_{0.45}Ga_{0.55}As$ barriers. The maximum indium concentration in the graded buffer is 34%. For the well doped case, the entire well is doped, whereas for the barrier doped case, we have 10Å undoped, 10Å doped, 10Å undoped, 10Å doped, and 10Å undoped. The barriers were doped such that the sheet charge density would be the same as in the lowest three well doped cases. For the barrier doped samples, we see that with increased doping, band bending results in a decrease in the absorption energy.

It is interesting to note that the IAF, rises steadily with the doping for the lower doping concentrations. Also, all three geometries, TM, TE and NI, behave the same. However, for the higher doping concentrations, the TE and NI geometries, in which the electric field is contained entirely in the plane of the QWs, the IAF begins to decrease. On the other hand, in the TM geometry, where we also have a component of the electric field in the direction of growth, the IAF continues to rise. The difference in behavior between the TM and TE/NI cases may be due to a difference in the joint density of states. In all cases, we found the FWHM to be on the order of 60–85 meV, where, in general, it was narrower for the barrier doped samples.

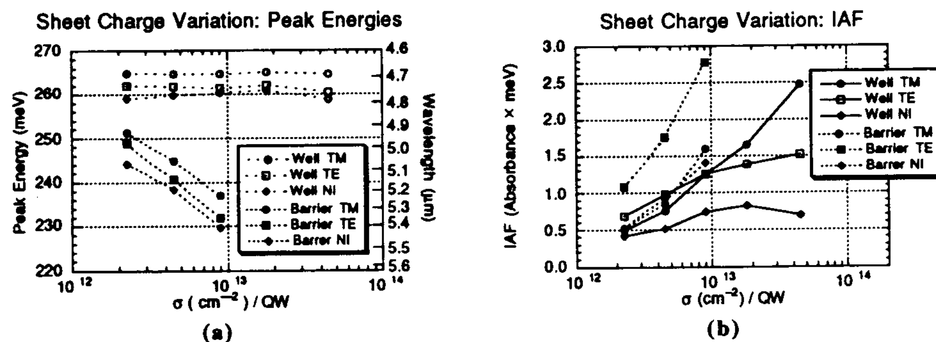

Figure 4

a) Peak energies and b) IAF for various doping concentrations (per QW) for TM, TE and NI orientations. The doping is either throughout the wells or in the barriers. The wells are 45Å $In_{0.50}Ga_{0.50}As$ with 50Å $Al_{0.45}Ga_{0.55}As$ barriers.

3. Second Harmonic Generation in Asymmetric Quantum Wells

QW intersubband nonlinear effects have been widely demonstrated in the 8–12µm regime[18] showing much stronger susceptibilities than their bulk counterparts. Resonant HIC–QW structures could develop into mid-infrared nonlinear devices if they show sufficient susceptibilities at the wavelength of an available source of radiation (solid state laser sources for example). However, as the QW system presents resonant absorption close to the nonlinear susceptibility maximum, both linear and nonlinear spectra have to be known accurately in order to calculate the figure of merit of any device[19]. Optical spectroscopy of optimized QW

structures can provide a test for the simple models of the susceptibilities. We report second harmonic generation (SHG) of light at 2.5 µm from a nearly doubly resonant (5.5–3µm) $Al_{0.45}Ga_{0.55}As/In_{0.50}Ga_{0.50}As$ step multi–QW structure. The spectral behavior of the susceptibility $\chi^{(2)}$ of the QW epilayer is measured as a function of detuning, by an interference method, using the second harmonic electric field generated from the GaAs substrate [20, 21].

3.1. DOUBLY RESONANT QUANTUM WELL STRUCTURE

SHG in n–type QWs have been reported in the 10µm region[18, 19, 22], in which non inversion symmetry is achieved by applying an electrical bias on a square well[23] or growing compositionally asymmetric QWs (step wells[22, 24] or coupled QWs[25] for example). The SHG susceptibility can be expressed in that case as[26]:

$$\chi^{(2)}_{QW} \propto \sum_{m,n} \frac{z_{1n} \times z_{nm} \times z_{m1}}{(\hbar\omega - E_{1n} - i\,\Gamma_{1n}) \times (2\,\hbar\omega - E_{1m} - i\,\Gamma_{1m})} \tag{1}$$

where z_{mn} are dipole matrix elements of the transition between the m and n QW envelope states, E_{mn} the intersubband energy and Γ_{mn} is the dephasing energy. Doubly resonant quantum wells were reported to present the highest SHG susceptibility, for which the dominant term of (1) corresponds to $n = 2$ and $m = 3$. The design of a quantum well showing maximum susceptibility consists of achieving both maximum dipole matrix element product $z_{12} \times z_{23} \times z_{31}$ by designing the well shape, together with a minimum in the denominator. The latter consideration consists of achieving a double resonance and minimum dephasing terms for a given targeted transition energy. This can be done by adjusting the growth parameters[15].

3.1.1 Sample optimization

Our sample was grown by molecular beam epitaxy on a (100) GaAs wafer, using an InGaAs graded buffer[1]. The asymmetric step quantum well (ASQW) structure consists of 50 periods of a 39Å $In_{0.54}Ga_{0.46}As$ and 31Å $In_{0.24}Ga_{0.76}As$ QW separated by 80Å $Al_{0.45}Ga_{0.55}As$ barriers, as shown on figure 5.

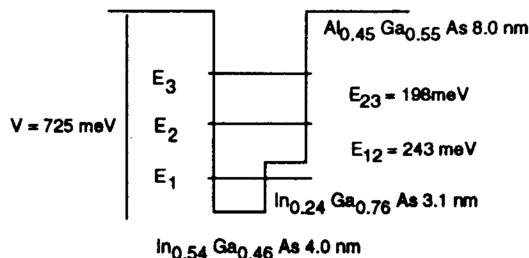

Figure 5.
Conduction band diagram of the asymmetric step quantum wells used in this study.

The quantum well is *n*–doped to 2.9×10^{12} cm^{-2} in the high indium section of the well. Maximum conduction band discontinuity was 725meV allowing in principle, resonances as high as 3µm. The well was designed to be doubly resonant around 6µm.

3.1.2 Linear spectrum and Calculation of $\chi^{(2)}$ of the QW structure

The absorption spectrum of the structure was measured with a FTIR spectrometer, the sample being at Brewster's incidence angle and the light TM polarized. We used a proton bombarded sample as a reference[14]. The normalized spectrum of absorption per quantum well is plotted on Figure 6a. A strong intersubband absorption is observed at 227meV (5.5µm) with a FWHM of 25meV corresponding to the 1–2 transition. The measured IAF is 27 mAbs-meV-per-QW. A smaller feature corresponding to the 1–3 transition is observed at 412meV (3.0µm) with a FWHM of 42meV and a IAF of 2.9 mAbs-meV / QW.

From the absorption spectrum we can extract the intersubband energies (E_{12} = 227meV, E_{13} = 412meV) and linewidths (Γ_{12} = 12.5meV, Γ_{13} = 21meV) for the transitions 1–2 and 1–3. One can note that the 1–2 transition is resonant at 5.5µm and the 1–3 at 3µm which means that the double resonance criterion is only approximate for this structure. We will ıssume an effective doping of 1.45×10^{12} cm^{-2} per QW in subsequent calculations of nonlinear susceptibilities, corresponding to the measured IAFs. We then assume the dipole matrix elements as calculated with a single band model[27], taking into account band non-parabolicity[4, 5]: z_{12}= 16.4 , z_{23} = 19.3, z_{13} = 2.52 Å. The $\chi^{(2)}$ deduced from (1) is shown on figure 6b, together with the two terms of the denominator of the dominant component, in absorption units.

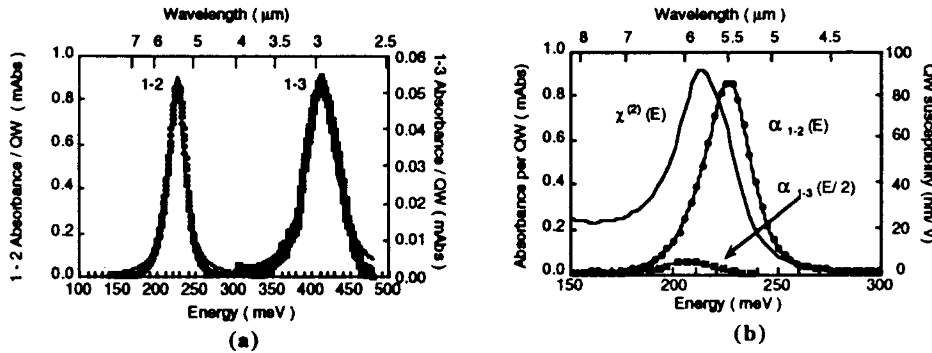

Figure 6

Absorption spectrum of the step quantum well sample (a). Simulated susceptibility and linear resonances leading to it in absorbance units (b)

The resonance of $\chi^{(2)}$ is close to 6µm with a value of 130nm / V as compared to the 5.5µm resonant absorption because the energy of the 1–3 transition is less than twice that of the 1–2 transition. $In_{0.60}Ga_{0.40}As/AlAs$ asymmetric coupled QWs have also been optimized for maximum $z_{12}\times z_{23}\times z_{31}$ and minimum linewidth. The absorption spectrum demonstrates exact .–?µm double resonance[5]. The simulated $\chi^{(2)}$ was about 150nm/V, about 100 times larger than the $\chi^{(2)}$ of bulk GaAs (180pm/V)[28], already a good nonlinear material.

3.2. $\chi^{(2)}$ MEASUREMENTS

3.2.1 Interference measurements

On the HIC–QW structure grown on GaAs, both the epilayer ($\chi^{(2)}_{QW}$) and the substrate ($\chi^{(2)}_{GaAs}$) are sources of SHG. The extraction of $\chi^{(2)}_{QW}$ makes use of the interference between the GaAs and multilayer generated second harmonic electric fields [20, 21]:

$$E(2\omega) = \left(\chi^{(2)}_{GaAs} + \chi^{(2)}_{QW}(\omega)\right) E(\omega)\, E(\omega) \tag{2}$$

Figure 7 shows the geometry of the experiment. The light enters the sample with an incidence angle, ϑ (internal angle r), and an angle φ between the (110) direction of the GaAs substrate and the plane determined by the direction (001) and the polarization of the incident electric field, as shown. A harmonic electric field builds up from the epilayer QW over a length L_{QW} (= 0.6μm). Then a harmonic electric field is generated from the GaAs substrate. The substrate of length L being many coherence length long (l_c is a few tens of microns in the mid IR). Thus energy flows back and forth between the fundamental and harmonic waves[26]. Our SHG signal measured after the sample is then a coherent superposition of those two effects.

For comparable values of the susceptibilities $\chi^{(2)}_{GaAs}$ and $\chi^{(2)}_{QW}$, the SHG signal from the bulk overwhelms that of the epilayer, by a factor given by the ratio of the lengths in which the radiation is generated. However, the symmetry and electronic structures of the bulk and epilayer region are different: $\chi^{(2)}_{GaAs}$ and $\chi^{(2)}_{QW}$, have different non-zero elements *(zzz)* and *(xyz)* respectively, so that polarization selection leads to measure either a coherently superimposed signal or only the GaAs generated signal. For the parallel polarization configuration, the SHG conversion can be expressed as[19]:

$$\frac{I_{2\omega}}{I_{\omega}^{2}} = T(\vartheta) \left| \chi^{(2)}_{GaAs}\, L\, G_{xyz}(r, \varphi) . \left(1 - e^{-2i\zeta}\right) + \chi^{(2)}_{QW}(\omega)\, L_{QW} F_{zzz}(r) \right|^{2} \tag{3}$$

where $I_{2\omega}$, and I_{ω} are the harmonic and fundamental power densities. $T(\vartheta)$ is the Fresnel transmission of the ω and 2ω electric fields at the sample interfaces and G_{xyz} and F_{zzz}, stand for the projection of electric fields on the principal axes of the crystal. The phase difference, ζ, between the ω and 2ω electric fields after the sample, can be expressed as:

$$\zeta = \frac{\pi}{2} \frac{L}{2\, l_c \cos r} \tag{4}$$

The extraction of $\chi^{(2)}_{QW}$ consists of fitting ζ and the complex $\chi^{(2)}_{QW}$ from Eq. (3) for the SHG measured for different polarization configurations. This provides both amplitude and phase information if the phase difference ζ were known with sufficient accuracy. The value of the coherence length is calculated[26] from the measured value of the GaAs indices in the mid-infrared[29].

3.2.2 Experimental arrangement

The experiment was performed with the Free Electron Laser in the Stanford FEL Center[2], which emits light micropulses of about 2 picoseconds (energy 0.5μJ) at a repetition rate of 11.8MHz and at a wavelength continuously tunable between 3.5 and 6.5μm. The laser beam arriving in the experimental area, was split between a sample channel and reference channel (Figure 8) and focused to a beam diameter of 100μm with parabolic reflectors on both the QW sample and a $AgGaSe_2$ crystal. The SHG signal from the $AgGaSe_2$ crystal was used to monitor micropulse power fluctuations.

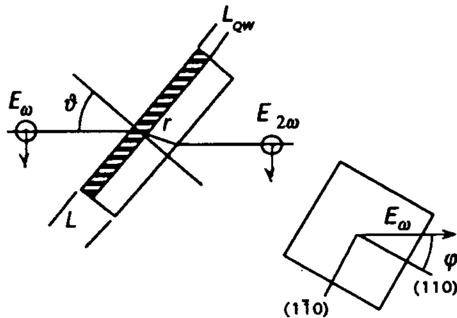

Figure 7
Geometry of the experiment.

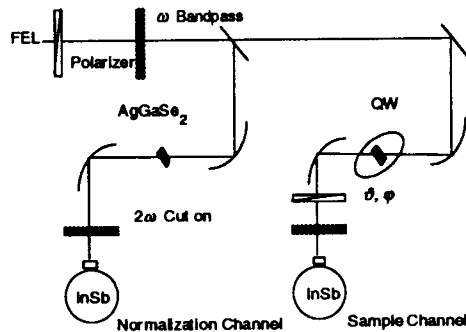

Figure 8
Layout of the SHG experiment.

Linear polarization of the incident beam is selected, and the laser harmonics are removed by an interferometric filter. The sample consists of either the QW sample or a proton bombarded version of it, where no carriers are available for excitation, so that $\chi^{(2)}_{QW}$ is null. The latter sample provides a normalization of the susceptibilities to that of GaAs.

3.2.3 Results

Figure 9 shows the scans obtained when φ is varied for three different wavelengths and for a SHG polarization parallel to that of the fundamental light beam. The 6.3, 5.4 and 5.1μm wavelengths have been chosen so that the SHG signal generated from the GaAs is a maximum. Coherence lengths of 77, 60, and 49μm are obtained from the best Sellmeier fits of measured refractive indices known with 10^{-3} accuracy[29]. The substrate thickness is measured to be 514μm both directly and deduced from Fabry Perot oscillations measured with a FTIR spectrometer. This thickness is then 7, 9 or 11 times l_c at the respective wavelengths.

According to Eq. (3), as the angle φ is varied, the SHG from a proton bombarded sample yields 4 even peaks following a $\cos^2 2\varphi$ dependence. This arises from the pure contribution of GaAs, as seen in figure 9a, at 6.3μm. A best fit of the experimental data is given as well, in which the only fitting parameter is the ratio of measured SHG to susceptibility of GaAs, taken as 180pm/V[28].

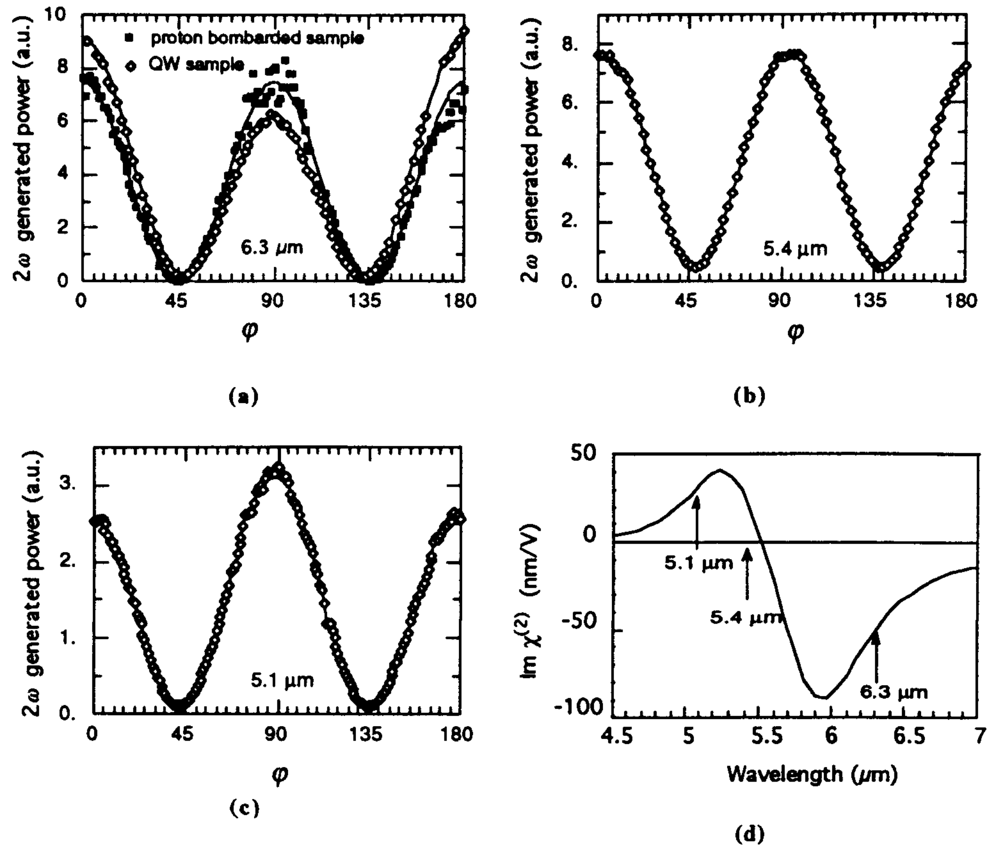

Figure 9

Variation of the SHG power as a function of φ angle for original and proton bombarded samples at 6.3μm.(a) Variation of the SHG power as a function of φ angle for original sample at 5.4 (b) and 5.1μm. (c). The spectrum of the imaginary part of $\chi^{(2)}{}_{QW}$ using a simple perturbative model (parameters from absorption spectrum) is presented (d).

Figure 9a also shows the variation of the SHG power with angle φ arising from the unprocessed sample, at an incidence angle of 65°. Two features are noted: (1) an unevenness between the 0°, 180° peaks and 90°, 270° peaks, and (2) a DC baseline of the SHG. According to Eq. (3), the unevenness of the peaks comes primarily from the imaginary part of $\chi^{(2)}{}_{QW}$ if we assume that the wafer thickness is close to an odd multiple of coherence lengths at this wavelength. With the same assumption, the DC offset arises primarily from the real part of the $\chi^{(2)}{}_{QW}$. A best fit of the φ scan is given assuming the value of 77μm for l_c at 6.3μm. The only two fit parameters are the imaginary and real part of $\chi^{(2)}{}_{QW}$. The accuracy of the result is strongly dependent on the assumed value of l_c. An accuracy of 10^{-3} for the indices does not allow accurate deduction of the amplitude of the real and imaginary parts of

$\chi^{(2)}_{QW}$. Direct measurements of the coherence length are also performed using a wedged[20] GaAs sample to increase the accuracy of l_c. In our present knowledge of the coherence length at that wavelength, the imaginary part of $\chi^{(2)}_{QW} = -30$nm/V (±50%) is deduced.

The same measurements were also performed at 5.4 and 5.1μm, as shown in figure 9b and 9c. The non uniformity of the peaks changes from higher 0° and 180° peaks, to even peaks, to higher 90° and 270° peaks for 6.3, 5.4, and 5.0μm respectively. Assuming a phase mismatch ζ of respectively $\pi/2$, $-\pi/2$ and $\pi/2$ as deduced from the values of the coherence length l_c, we can infer that the imaginary part of the $\chi^{(2)}_{QW}$ goes from negative to null and then to positive respectively. This feature in the variation of Im $\chi^{(2)}_{QW}$ is consistent with the spectrum calculated from the perturbation development (resonant and non resonant terms)[26] as shown in Figure 9d, in which the values of intersubband energies and dephasing terms were fit from the absorption spectrum of the sample.

We notice on figure 9b that the DC offset is maximum at 5.4μm where the imaginary part of $\chi^{(2)}_{QW}$ is null. We can deduce a magnitude of 70nm/V for the $\chi^{(2)}_{QW}$ at this wavelength. Better accuracy of l_c is needed in order to extract both the real part and the magnitude of the susceptibility. Incidence angle, ϑ, variations of the SHG are consistent with the values extracted from the φ scans. Spectrally resolved measurements of $\chi^{(2)}_{QW}$ are in progress on other optimized structures.

4. Conclusion:

We have shown normal incidence absorption from heavy hole to light hole states. Variation of barrier thickness was found not to effect the transition energy, but only the strength of the absorption. Width and doping variation studies were also conducted. The maximum intravalence band transition energy was found to be 300meV (= 4.13μm) in the 27Å well. Higher IAFs were found in barrier doped samples, though the transition energy decreased due to band bending. In the conduction band, SHG of 2.5μm light was demonstrated using a HIC asymmetric step QW with intersubband resonances corresponding to photons of wavelength 5.5 and 3.1μm. $\chi^{(2)}_{QW}$ measurements were performed at 6.3, 5.4 and 5.1μm. The largest susceptibility we measured, was 70nm/V at 5.4μm. A sign reversal of a $\chi^{(2)}$ is demonstrated in a QW system for the first time. By demonstrating normal incidence absorption at 4.1μm in the valence band and second harmonic generation of 2.5μm light in the conduction band, we have shown that the high Indium content quantum well (HIC-QW) system is promising for mid-IR applications.

Acknowledgements:
E. Martinet acknowledges fellowship support from the Office of Naval Research (ONR) and Lockheed, and H.C. Chui from an ONR Fellowship. This work was supported by ONR under contract N00014-91-J-0170 and N00014-92-J-1903 and by ARPA under contract N00014-90-J-4056. FTIR measurements were performed on a Bruker FTIR at the Stanford Free Electron Laser facility.

References:

1. Lord S M, Pezeshki B, Harris J S Jr. *Investigation of High In Content InGaAs Quantum Wells Grown on GaAs by Molecular Beam Epitaxy.* Electronics Letters 1992;**28**(13):1193-1195.

2. Smith T I, Schwettman H A, Berryman K W, Swent R L. *Facilities at the Stanford Picosecond FEL Center.* In: Schwettman HA, ed. *Free Electron Laser spectroscopy in Biology, Medicine, and Material Science.* Los Angeles, CA: , 1993: 23.

3. Chui H C, Lord S M, Martinet E, Fejer M M, Harris J S Jr. *Intersubband transitions in high indium content InGaAs/AlGaAs quantum wells.* Appl. Phys. Lett. 1993;**63**:364.

4. Chui H C, Martinet E, Fejer M M, Harris J S Jr. *2.1μm wavelength intersubband transitions in InGaAs / AlGaAs quantum wells.* Appl. Phys. Lett. 1993;.

5. Chui H C, Martinet E L, Fejer M M, Harris J S Jr. *Large energy intersubband transitions in high Indium content InGaAs / AlGaAs quantum wells,.* In this volume.

6. Kane E O. *Band structure of indium antimonide.* J. Phys. Chem. Solids 1956;**1**:249.

7. Levine B F, Gunapala S D, Kuo J M, Pei S S, Hui S. *Normal incidence hole intersubband absorption long wavelength GaAs/$Al_xGa_{1-x}As$ quantum well infrared photodetectors.* Appl. Phys. Lett 1991;**59**(15):1864.

8. Park J S, Karunasiri R P G, Wang K L. *Intervalence-subband transition in SiGe/Si multiple quantum wells—normal incident detection.* Appl. Phys. Lett. 1992;**61**(6):681-683.

9. Katz J, Zhang Y, Wang W I. *Normal incidence intervalence subband absorption in GaSb quantum well enhanced by coupling to InAs conduction band.* Appl. Phys. Lett. 1993;**62**(6):609-611.

10. Karunasiri R P G, Park J S, Wang K L. *Normal incidence infrared detector using intervalence-subband transitions in $Si_{1-x}Ge_x$/Si quantum wells.* Appl. Phys. Lett. 1992;**61**(20):2434-2436.

11. Xie H, Katz J, Wang W I. *Infrared absorption enhancement in light- and heavy-hole inverted $Ga_{1-x}In_xAs/Al_{1-y}In_yAs$ quantum wells.* Appl. Phys. Lett. 1991;**59**(27):3601.

12. Gunapala S D. *InGaAs/InP hole intersubband normal incidence quantum well infrared photodetector.* J. Appl. Phys. 1992;**71**(5):2458.

13. Indium concentrations were determined by high resolution X-ray diffraction measurements on a separate sample grown at the time of the other growths.

14. Yoo S J B, Fejer M M, Byer R L, Harris J S Jr. *Second Order Susceptibility in Asymmetric Quantum Wells and its Control by Proton Bombardment.* Appl. Phys. Lett. 1991;**58**(16):1724-1726.

15. Chui H C, Harris J S Jr. *Growth Studies of $In_{0.5}Ga_{0.5}As$/AlGaAs Quantum Wells Grown on GaAs with a Linearly Graded InGaAs Buffer.* submitted to: J. Vac. Sci. Tech. B .

16. Andreani L C, Pasquarello A, Bassani F. *Hole subbands in strained GaAs-$Ga_{1-x}Al_xAs$ quantum wells: Exact solution of the effective-mass equation.* Phys. Rev. B 1987;**36**(11):5887.

17. O'Reilly E P, Witchlow G P. *Theory of the hole subband dispersion in strained and unstrained quantum wells.* Phys. Rev. B 1986;**34**(8):6030.

18. Bibliography Rosencher E, Vinter B, Levine B, ed. *Intersubband Transitions in Quantum Wells.* London: Plenum, 1992:345. ; vol 288).

19. Yoo S B J. *Linear and Nonlinear Spectroscopy of Quantum Well Intersubband Transitions* [Stanford University Thesis]. Stanford, 1991.

20. Wynne J J, Bloembergen N. *Measurement of the lowest-order nonlinear susceptibility in III-V semiconductors by second-harmonic generation with CO2 laser.* Phys. Rev. 1969;**188**(3):1211.
21. Hollering R W J. *Bulk and surface second-harmonic generation in noncentrosymmetric semiconductors.* Optics Comm. 1992;**90**:147.
22. Rosencher E, Bois P, Nagle J, Delaître S. *Second harmonic generation by intersubband transitions in compositionally asymmetrical MQWs.* Electron. Lett. 1989;**25**:1063.
23. Fejer M M, Yoo S J B, Byer R L, Harwit A, Harris J S Jr. *Observation of extremely large quadratic susceptibility at 9.6 - 10.8 μm in electric-field-biased quantum wells.* Phys. Rev. Lett. 1989;**62**:1041.
24. Boucaud P, Julien F H, Yang D D, et al. *A detailed analysis of second harmonic generation near 10.6 μm in GaAs/AlGaAs asymmetric quantum wells.* App. Phys. Lett. 1990;:(in the press).
25. Capasso F, Sirtori C, Sivco D, Cho A Y. *Nonlinear Optics of Intersubband Transitions in AlInAs/GaInAs Coupled Quantum Wells: Second Harmonic Generation and Resonant Stark Tuning of* $\chi_{2\omega}^{(2)}$. In: Rosencher E, Vinter B, Levine B, ed. Intersubband Transitions in Quantum Wells. New York: Plenum, 1992: 141-9.
26. Shen Y R.*The Principles of Nonlinear Optics*.New York: Wiley, 1984
27. Bastard G, Delalande C, Ferreira R, Liu H W. *Assisted relaxation and vertical transport of electrons,holes and excitons in semiconductor heterostructures.* J. Lumin. 1989;**44**:247.
28. Levine B F, Bethea C G. *Non linear susceptibility of GaP: Relative Measurement and Use of Measured Values to Determine a Better Absolute Value.* Appl. Phys. Lett. 1972;**20**:272.
29. Pikhtin A N, Yas'kov A D. *Dispersion of the refractive index of semiconductors with diamond and zinc-blende structures.* Sov. Phys. Semicond. 1978;**12**(6):622.
30. Zhang Y, Baruch N, Wang W I. *Normal incidence infrared photodetectors using intersubband transitions in GaSb L-valley quantum wells.* Appl. Phys. Lett. 1993;**63**(8):1068